

The Power of Alignment-Free Histogram-based Functions: a Comprehensive Genome Scale Experimental Analysis - Version 1

Giuseppe Cattaneo^{*†} Umberto Ferraro Petrillo^{‡*} Raffaele Giancarlo[§]
 Francesco Palini^{*} Chiara Romualdi[¶]

Abstract

Motivation: Alignment-free (AF, for short) distance/similarity functions are a key tool for sequence analysis. Experimental studies on real datasets abound and, to some extent, there are also studies regarding their control of false positive rate (Type I error). However, assessment of their power, i.e., their ability to identify true similarity, has been limited to some members or variants of the D_2 family and the asymptotic theoretic results have been complemented by experimental studies on short sequences, not adequate for current genome-scale applications. Such a State of the Art is methodologically problematic, since information regarding a key feature such as power is either missing or limited.

Results: By concentrating on histogram-based AF functions, we perform the first coherent and uniform evaluation of the power of those functions, involving also Type I error for completeness. The experiments carried out are extensive, as we use two Alternative models of important genomic features (CIS Regulatory Modules and Horizontal Gene Transfer), sequence lengths from a few thousand to millions and different values of k . As a result, and using power, we provide a characterization of those AF functions that is novel and informative. Indeed, we identify weak and strong points of each function considered, which may be used as a guide to choose one for analysis tasks. In synthesis, and quite remarkably, of the fifteen functions that we have considered, only four stand out. Finally, in order to encourage the use of our methodology for validation of future AF functions, the Big Data platform supporting it is public.

1 Introduction

Alignment-free distance/similarity functions (AF functions, for short) provide an alternative approach to traditional sequence alignment methods, e.g., [1, 13], for determining how distant/close two sequences are. Their advantages/disadvantages with respect to alignment methods are well presented in [19].

Although AF functions have a long and established history [17] and their use has been widely investigated for sequence analysis in genomics [16, 19], metagenomics [2], and epigenomics [5, 6], only recently a comprehensive experimental study on benchmark and real datasets has appeared in the Literature [19]. It has been followed by another study, as an application of the Big Data platform FADE [4], in which Type I error control has been determined for some prominent AF functions, providing additional information with respect to the benchmarking study since it has been performed on the same real datasets.

However, for a full assessment of the “value” of an AF function, its power, i.e, its ability to identify true positives, must also be estimated. Unfortunately, those studies are scarce and confined to the D_2 family of AF functions or variants. Power estimation has been investigated theoretically in [18] and experimentally, exclusively [7, 12] or mostly [10], on synthetic datasets. Indeed, as opposed to Type I error control studies, power studies are less amenable to be performed on real datasets, where they may provide inaccurate results,

^{*}Dipartimento di Informatica, Università di Salerno, Fisciano (SA), 84084, Italy

[†]To whom correspondence should be addressed.

[‡]Dipartimento di Scienze Statistiche, Università di Roma - La Sapienza, Rome, 00185, Italy

[§]Dipartimento di Matematica ed Informatica, Università di Palermo, Palermo, 90133, Italy

[¶]Dipartimento di Biologia, Università di Padova, Padova, 35131, Italy

as reported in [10]. Therefore in agreement with the indication of that study we resort to use simulated datasets. It is to be highlighted that there is also a subtle connection between power and Type I error control. Indeed, a high power may be determined by a poor Type I error control. As a consequence, although Type I error control studies for AF functions are now available on benchmark real datasets [4], we repeat them here on synthetic datasets for completeness. We also adhere to the ground-breaking methodology proposed in [12]. In particular, we use two models of “biologically relevant ” similarity, one resulting from the process of horizontal gene transfer and the other resulting from the process of acquiring common CIS regulatory elements [7, 10, 12]. The first is referred to as Alternative model Pattern Transfer and the second as Motif Replace.

Being the range of experiments we perform here much broader than those of [10, 12], here we present the first extensive study of the power of AF functions by concentrating on histogram-based ones [11]. They use *k-mer statistics* statistics, and our choice is due to their simplicity, effectiveness and widespread use, as documented by a recent benchmarking study [19]. We have chosen the best performing histogram-based AF functions according to the mentioned benchmarking, representatives of all types of AF functions described in [11]. Our results are as follows.

- Histogram-based AF functions assure a good Type I error control. That is, in a “neutral environment” where randomly generated pairs of sequences are intentionally labeled as similar, the functions are difficult to fool. As shown [4] when using real datasets Type I error control is more heterogeneous across AF functions.
- Our power studies provide a novel classification of histogram-based AF functions much more informative than the standard taxonomic one, i.e, the one provided in [11] (see also [3]). Briefly, we identify a handful of functions that stand out in terms of performance and we advance the knowledge regarding the power of the prominent and much studied D_2 family in relation to the two Alternative models.
- Our results indicate that the heuristic law commonly used for the selection of k , i.e., as the logarithm of sequence lengths, is generally not appropriate. In fact, for Type I error control, the choice of k seems to be marginal for a good performance, while it has a complex relation with Alternative model, sequence length and function. Differently from other studies, our work provides recommendations and guidelines regarding the most appropriate choice of k which is very much dependent on the function and its parameters.
- In order to encourage the use of our methodology for future benchmarking, we provide a new computational framework based on a succinct data structures Big data Platform, namely FADE [4], which guarantee the reproducibility of the entire methodology and that can be further extended with the user provided functions.

2 Methods

2.1 Distance Functions

The histogram-based AF functions chosen for this study are summarized in Section 1 of the Supplementary Material, together with their definitions. They all depend on the choice of k , i.e., the k -mer length used for the statistics. The heuristic for the selection of k is to choose as k the logarithm of the sequence length (see formula 56 in [11]). Here we select k as a set of values upper bounded by the logarithm of the maximum sequence length. Then, for the evaluation of AF function performance, we proceed combinatorially, i.e. the assessment is made for each combination of the chosen values of n and k .

2.2 The Methodology for the Experimental Study of Control of Type I Error and Power

A consolidated approach for the evaluation of the performance of a statistic, in our case an AF function, concerns the efficacy in discriminating random from real effects. The corresponding quantification is generally obtained by evaluating the control of Type I error and the power of the test statistic. This hinges on two main ingredients: Generative Models for simulating pairs of sequences and statistical test. The work by Reinert et al. [12] regarding the D_2 statistics is a clear instance of such a methodology that we closely follow, with the addition of providing public software and benchmark datasets.

Traditionally, the AF functions included in this study are grouped by mathematical families (see supplementary Material and [11, 3]). We anticipate that, in what follows, the functions belonging to the same family are listed contiguously in Tables and Figures, with no separation among families.

2.2.1 Generative Models for Sequences

Null Model. It is intended to formalize the generation of pairs of sequences “similar by chance”. Given an alphabet $\Phi = \{A, C, G, T\}$ with uniform probability distribution and two integers n and m , m pairs of sequences, each of length n , are generated using random samplings from a multinomial distribution $Multinom(p, n)$. In what follows, we refer to this model simply as *NM*.

Alternative Model: Pattern Transfer. This model, introduced in [12] and with variants proposed in [8, 14], is intended to capture the process of acquiring similarity between two biological sequences via horizontal gene transfer. Our model is essentially the same as the original one, and we describe it in parametric form.

Fix an integer ℓ , whose role will be clear immediately. First, m pairs of sequences are generated via $Multinom(p, n)$. Then, each pair (x, y) is made more similar as follows. For each position i of x (with $i = 1 \dots n$), we randomly sample from a Bernoulli distribution $Bern(\gamma)$ (γ success probability). In case of success at position i , the sub-sequence $x[i, i + \ell - 1]$ replaces the sub-sequence $y[i, i + \ell - 1]$ and the next sampled position is $i + \ell$ (the sequence that has been replaced is hereafter called motif and ℓ denotes its length).

The result is a pair of sequences (x, \hat{y}) , where \hat{y} is intuitively more similar than y to x . Such a similarity increases with the increase of the probability of success γ . Finally, the set of the new m pairs of (x, \hat{y}) is returned as output. We refer to this model as $PT(\ell, \gamma)$. Again, when it is clear from the context, we omit mention of its parameters.

Alternative Model: Motif Replace. This model has been also introduced in [12]. It is similar to PT , except for the selection and replacement of the motif. Two sequences (x, y) , generated by $Multinom(p, n)$, are made more similar by implanting a motif in both sequences in the positions selected by $Bern(\gamma)$. That is, rather than a pattern transfer, both sequences acquire a copy of the motif starting at the same position.

Although no motivation was given for this model, it intuitively represents the notion of similarity between sequences that share many Transcription Factor binding sites, and as pointed out in [7], it models the acquisition of common CIS Regulatory Modules. In order to better model the biology underlying process, we modify the model by using a set of motifs to implant rather than one. Formal details follow.

First, m pairs of sequences of length n are generated as in the case of PT . Second, we build a set M of d distinct motifs, each of length ℓ using a simple variant of NM (details left to the reader). The number d is chosen to respect the proportion used in [12] regarding the number of motifs available for insertion into a pair of sequences, with respect to their length. In that case, a single motif of length 5 for sequences of length up to $\hat{n} = 25\,000$ was used. Accordingly, taking as reference the maximum sequence length used in Reinert et al., we choose $d = \frac{n}{m\ell}$. Third, when a position i in a pair of random sequences (x, y) is chosen for replacement, a motif t is randomly sampled from M (with replacement) and it is copied in both $x[i, i + \ell - 1]$ and $y[i, i + \ell - 1]$. We refer to this model as $MR(d, \ell, \gamma)$. Again, when it is clear from the context, we omit mention of its parameters.

2.2.2 Alternative vs Null Models: the Ability to Capture Similarity Trends

To fix ideas, we present the case of similarity functions, since the case of distances is analogous. Independently of whether or not a similarity function D is based on alignments, ideally, it has to be able to separate, in terms of its value, “truly” similar sequences from those that are not. In practice, it is able to capture such a separation in terms of a trend, rather than exactly, in a dataset of pairs of sequences. That is, a similarity trend in the data is captured in terms of a separation one.

The “comparison” of Alternative models with respect to Null ones allows for the quantification of how well a function captures those trends. The method we propose for such a quantification follows using, to fix ideas, NM and PT with parameter γ .

- (1) Generate a set S of m pairs of sequences, each of length n , via NM . Using S , generate a set S_γ of m pairs of sequences, each of length n , via PT with parameter γ .
- (2) Compute D for each pair of sequences in S and S_γ , respectively, and in agreement with the function parameters, e.g., k .
- (3) AF values computed in (2) are reported as boxplots and also as delta values, i.e differences between AM and NM average values, those latter in the form of heatmaps.

It is to be pointed out that S_γ can be computed with different values of γ . It is expected that a good similarity function would return large delta and non-overlapping boxplots, with the ones of S_γ “higher” than those of S .

2.2.3 Type I Error Control and Statistical Power

Given an AF function, all the statistical tests we perform in this study, and detailed in the following sub-sections, are based on the same inferential hypotheses: H_0 , the two sequences are similar by chance (Null hypothesis) and, H_1 , the two sequences are more similar than they would be by chance (Alternative hypothesis). Given our generative models, NM is used to define the null distribution, while PT and MR are used to generate pairs of similar sequences (the true positive pairs).

Given a nominal level α (Type I error), for each pair of sequences generated by NM , PT or MR , we estimate the number of sequence pairs for which a given AF function has a value more extreme than the percentile α of the null distribution (that is, we reject the H_0). If sequence pairs are generated with the NM model (sequences are similar by chance) the rejection of H_0 identifies a false positive, otherwise if sequence pairs are generated with AM , we identify a true positive.

Under H_0 , with a nominal level of α , the expected fraction of false positives obtained by chance is α . Then, a statistical test with a reasonably good control of Type I error, has a false positives rate close to the nominal level α .

On the other hand, the power of a statistical test is defined as the probability of correctly rejecting H_0 , i.e. a true positive is found. That is, letting β be the probability of not rejecting H_0 when it is false, the power of a test statistic is $1 - \beta$.

Here, to evaluate the statistical power of an AF measure, sequences are generated separately with PT or MR and tested on the null distribution, via NM . In this case, higher the number of sequence pairs identified as significantly similar is, higher the power.

2.3 Benchmarking Software and Datasets

The following tools, used for this research, have been made publicly available.

- **Datasets Generation.** We provide a Spark-based distributed tool for the automatic generation of collection of genomic sequences according to the types of Generative Models described in Section 2.2.1. The tool accepts as parameters the same ones as the models. Output sequences are encoded as standard FASTA files.

- **AF Function Evaluation.** An AF function between pair of sequences is evaluated using the FADE software (see [4]). It is a Spark-based distributed framework for AF analysis over large collections of genomic sequences, coming with the implementation of several popular AF functions. It rests on a multi-criteria succinct representation of k -mer dictionaries, well suited for effective storage and load balancing in a distributed setting.
- **AF Functions Analysis.** We provide a Java-based tool for estimating the Type I error rate and the power of the test statistic over a set of input AF functions, according to the methodology described in Section 2.2.3. This is done by comparatively analyzing the AF functions, evaluated over sequences generated according to the Null model, against the corresponding sequences generated according to the PT and MR Alternative models. Once available, these results are summarized and visualized using a proper graphical representation, by means of a collection of R scripts.

3 Results

3.1 Type I error control

For each AF function, we have estimated the Type I error rate, as specified in Section 2.2.3. The relevant parameters that specify the set of experiments carried out are as follows. We use 50 different sequence lengths n (starting from two hundred thousand to ten millions, with a step of two hundred thousands) and the number of pairs is $m = 1000$. The false positive rate has been estimated for $k = 4, 6, 8, 10$. For $\alpha = 0.05$, the percentage of false positives are reported cumulatively by length with boxplots in Figure 1. With the exception of the Chebyshev AF function, each AF function performs fairly well, since the values of the percentage of false positives is close to the nominal level α . For $\alpha = 0.01, 0.10$, the results are reported in Figure 1 of the Supplementary Material and we can draw a conclusion analogous to the one for $\alpha = 0.05$.

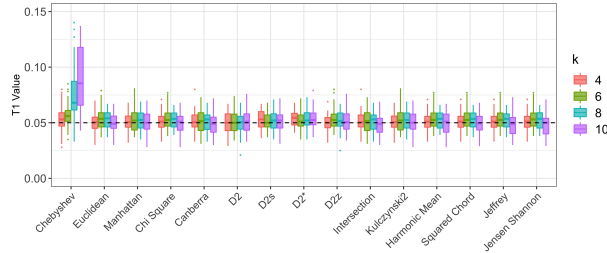


Figure 1: Results of the T1 Error Control experiments, nominal level $\alpha = 0.05$. For each AF function (x axis) and each value of k (left vertical color coding), the percentage of false positives over all lengths is represented by boxplots colored according to k . The dotted black line corresponds to the nominal level.

3.2 Ability to Capture Similarity Trends

Given a length $n = 5\,000\,000$, and a similarity/distance function, we generate 1000 sequence pairs and process them as reported in Section 2.2.2 for NM , PT , and MR with $\gamma = 0.01, 0.05, 0.1$, respectively.

In order to have an edit-based similarity/distance function as a reference point, we use the mentioned procedure with the Hamming distance (HD for short), being the most natural one to capture similarity as induced by our generative models. Results are reported in Figure 2 in terms of boxplots of HD values. We observe that, as expected, both PT and MR models generate sequence pairs with an increasing trend of similarity as γ values increase, with a very small level of variability. This is due to the fact that the two AM models produce highly similar sequences that have the same, perfectly aligned, number of common sub-sequences. It is also to be noted that the Hamming distance confirms that NM generates random sequences

with base probabilities equal to $1/4$. The delta values of HD clearly evident from Figure 2 guarantees that such a function is able to capture the increasing level of similarity between pairs of sequences produced by both PT and MR .

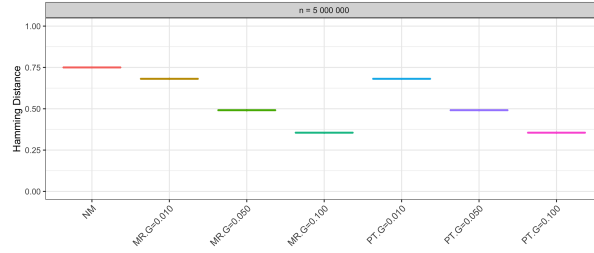


Figure 2: Separation, i.e., boxplots of HD values, providing a graphical view of the distance of values generated by the Alternative models, with respect to the Null model. The top indicates the value of n . On the x axis, the generative models considered, with the letter G denoting γ . For each experiment, the boxplot of the HD values computed on the corresponding set of pairs of sequences is reported on the y axis.

Moving from edit-based HD to histogram-based AF functions, we perform the same experiments with the same γ and n values, but with the addition of $k = 4, 6, 8, 10$. The results are reported in Figure 3 as heatmap of delta values (see Section 2.2.2). The dendrogram on the top of the figure is the result of a hierarchical clustering of AF function delta vectors using Euclidean distance and Complete Linkage clustering method [9].

In order to explain the clustering, we mention that colors in the heatmap encode the following situation, on a scale from red to blue: i) positive delta values (red colors) indicate that the AF function is able to capture the similarity with respect to the case of random sequences, i.e. higher the delta better the measure; ii) negative delta values (blue colors) indicate a complementary situation i.e. the measure is not able to capture the similarity.

Therefore, the clustering groups functions according to their ability to capture similarity.

Based on all the above, Figure 3 shows a global positive behaviour with the exception of Chebyshev and Canberra for the MR model. Apart from those two, the dendrogram groups AF functions into three clusters that we describe from right to left.

- The right side group (Euclidean, Manhattan, SquaredChord, χ^2 , Jeffrey, Jensen-Shannon) behave homogeneously well, independently of the Alternative models, but with some dependence of k and γ . That is, for $k = 4, 6$ this group captures similarity better than $k = 8, 10$, as γ increases. It is to be noted that Manhattan and Euclidean are the weakest in this group: smaller delta values (lighter red)
- The central group (D_2^S , Harmonic Mean, Intersection, Kulczynski2) is characterised by lower levels of delta, independently of the Alternative models, k and γ values.
- The leftmost group (D_2^* , D_2 , D_2z) shows the highest potential to capture similarities (highest delta values), especially for $k = 8, 10$. While D_2^* and D_2 seem to “prefer” MR , D_2z performs well in both Alternative models.

The previous analysis highlights AF average trends with an increasing similarity, but no quantitative information is provided regarding the ability of an AF function to identify truly similar sequences, i.e., true positives. Therefore, we resort to more rigorous power tests in the next section.

3.3 Power Estimation

3.3.1 Overall Classification

In order to evaluate statistical power of an AF measure, sequences are generated with PT or MR models and tested on the null distribution (obtained with the NM model). The estimation has been performed

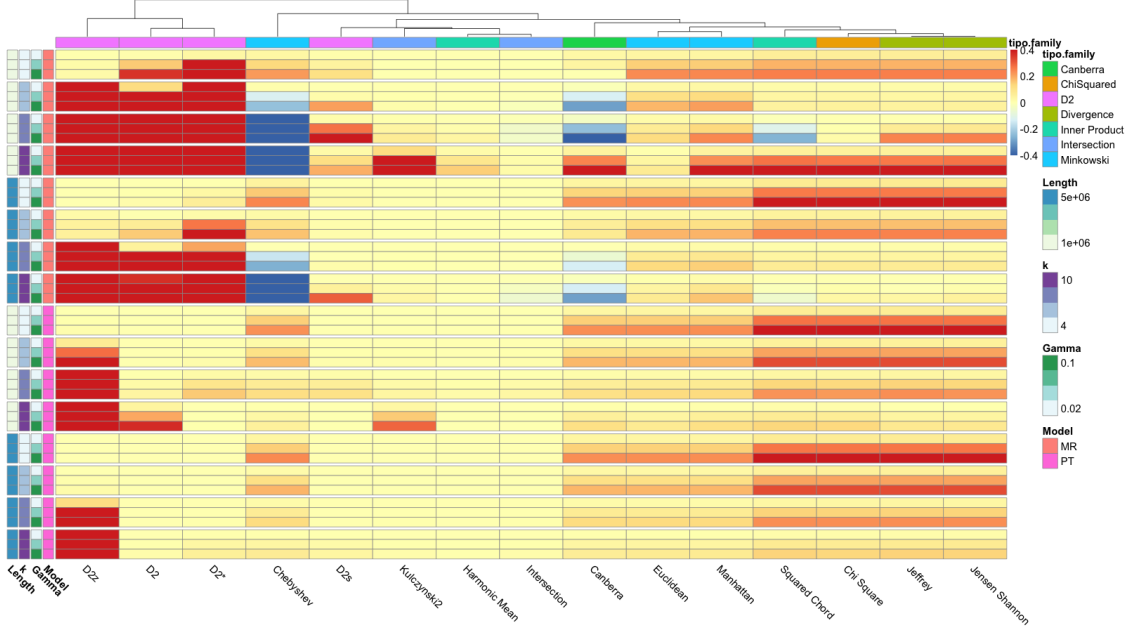


Figure 3: Ability to capture similarity trends. Heatmap of the delta values obtained as the difference between the average of the distribution of AF values computed with *NM* and one of *AM* and *PT*, for different combinations of k and γ and n (see main text), reported as colors on the left panel annotation. The dendrogram on the top is a hierarchical clustering on the delta values with Euclidean distance and Complete Linkage.

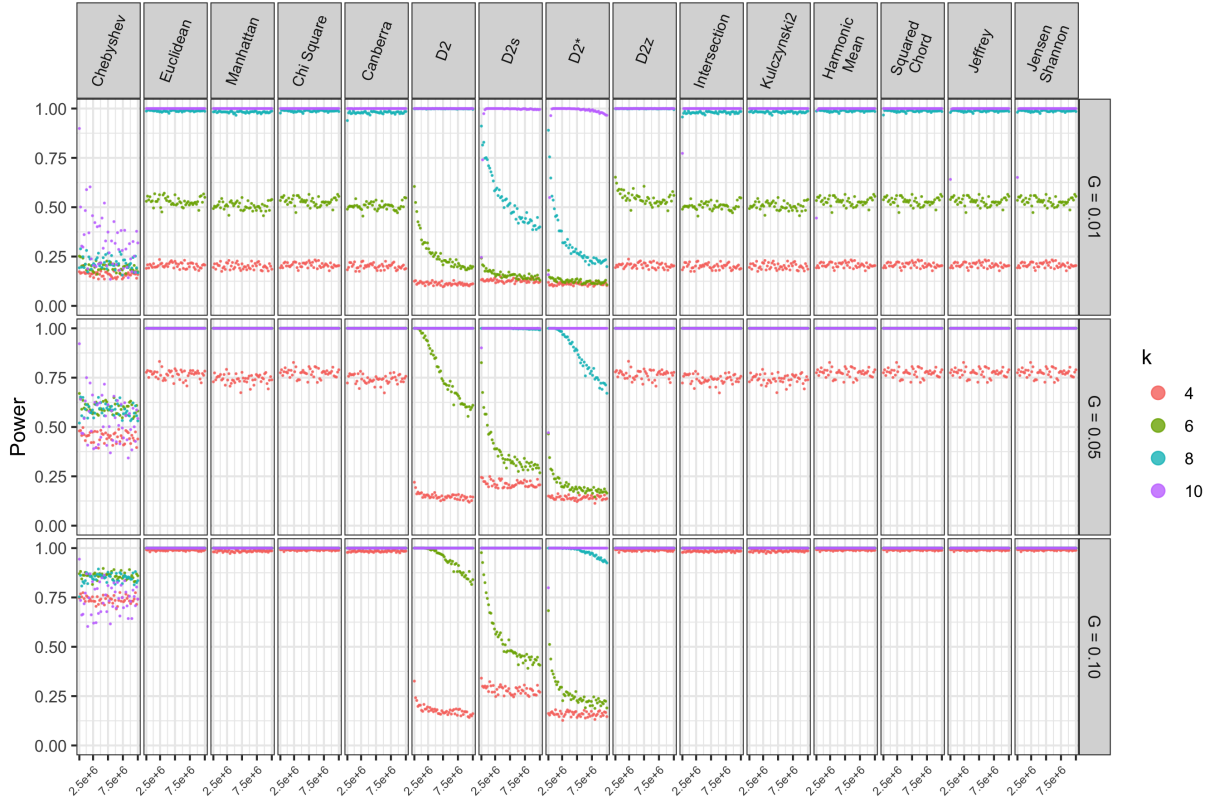
for the same n , k and α as reported previously (see Section 3.1), for both the *PT* and the *MR* Alternative models with the addition of $\gamma = 0.01, 0.05, 0.1$.

Supplementary Figure 4 reports the distribution of the proportion of true positives cumulatively by length. From that figure, in agreement with the trends depicted in Figure 3 for only one value of n , we find that AF power is k and Alternative models dependent. In addition, it has dependence on n . That is, i) as expected with the increasing similarity between sequences (from $\gamma = 0.01$ to $\gamma = 0.1$), we observe a general increase of the power; ii) $k = 4$ for our n range is characterised by a poor performance; iii) with some exceptions, $k = 8, 10$ show high power values; iv) in the *MR* model, Canberra, Intersection, Jeffrey, Jensen-Shannon, Squared Chord and D_2^S show a highly variable behaviour in terms of n and for $k = 8, 10$. Finally, the Chebyshev function is confirmed to be characterised by the worst performance in both models.

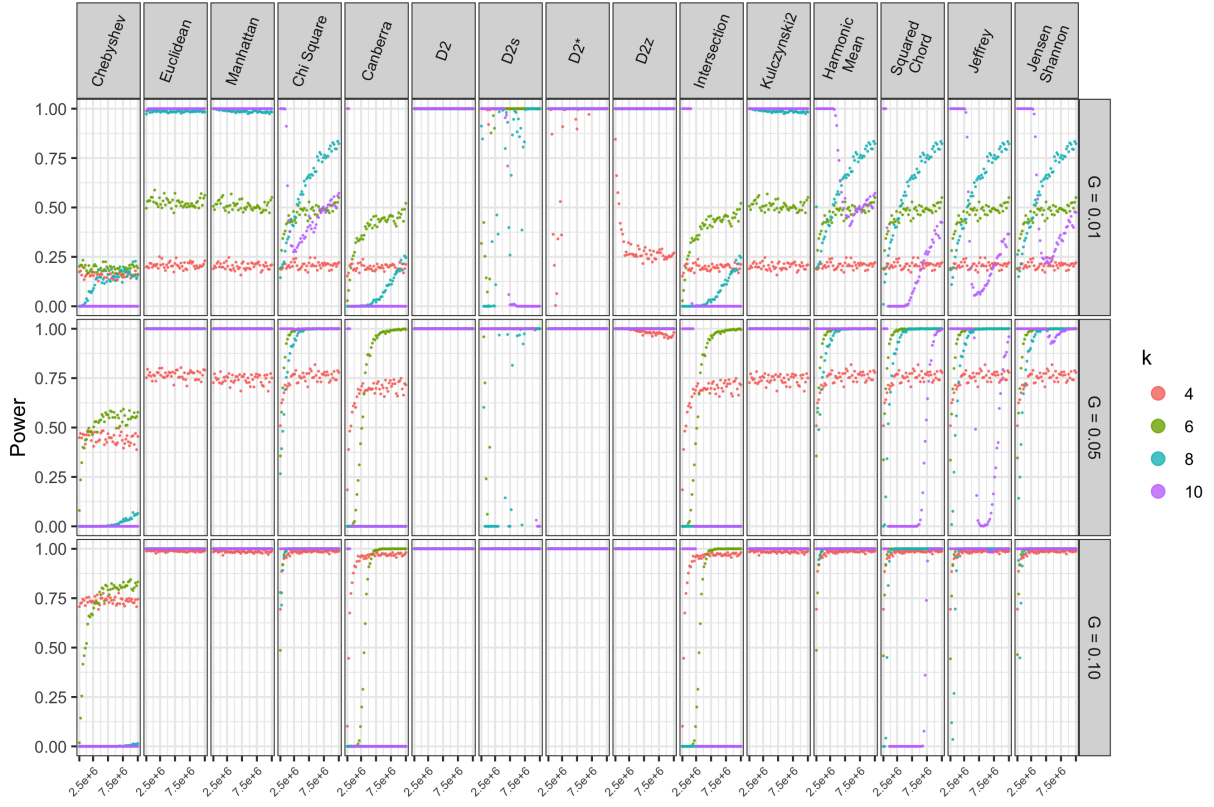
Figure 4 gives an even more accurate picture of the relationship among power, k , n and γ . We evidence some peculiar and unexpected power trends that allow us to classify AF function into two different groups: stable (when there is no functional relationship between power and n) and unstable (when on the contrary a clear increasing or decreasing trend can be observed between power and n). In particular, it allows to partition AF functions into four different classes, that we now define.

Class 1 has a stable power behaviour in both *MR* and *PT*; class 2 has a stable power behaviour in the *PT* but an unstable power behaviour in the *MR*; class 3 has a stable power behaviour in the *MR* but an unstable power behaviour in the *PT* and class 4 has an unstable power behaviour in both *MR* and *PT*. Those findings as reported in Table 1.

Unexpectedly, as reported in Figure 4, while in *MR* model most of the functional relationships between power and n show an increasing trend, in the *PT* model most of them are characterised by a decreasing trend (for $k = 6, 8$).



(a) Pattern Transfer



(b) Motif Replace

Figure 4: Power Analyses. Upper Panel: Power trend for the *PT* Alternative model. Lower Panel: Power trend for the *MR* Alternative model. For each AF and $\gamma = 0.01, 0.05, 0.1$ the power levels obtained across different values of n is reported and colored according to the value of k .

Table 1: Classification of the AF functions considered in this study according to their behavior in the *PT* and in the *MR* Alternative models.

AF Family	AF Method	PT	MR	CL
Minkowski	Chebyshev	unstable	unstable	4
Minkowski	Euclidean	stable	stable	1
Minkowski	Manhattan	stable	stable	1
χ^2	χ^2	stable	unstable	2
Canberra	Canberra	stable	unstable	2
D_2	D_2	unstable	stable	3
D_2	D_2^S	unstable	unstable	4
D_2	D_2^*	unstable	stable	3
D_2	D_2z	stable	stable	1
Intersection	Intersection	stable	unstable	2
Intersection	Kulczynski2	stable	stable	1
Inner Product	Harmonic Mean	stable	unstable	2
Inner Product	Squared Chord	stable	unstable	2
Divergence	Jeffrey	stable	unstable	2
Divergence	Jensen-Shannon	stable	unstable	2

3.3.2 Insights into the overall classification

Apart from AF functions belonging to class 4, the previous classification evidences that some AF functions previously characterized by a reasonable good ability to capture similarity trend (see Section 3.2), to a closer and more rigorous scrutiny show poor power at least in one model. In order to provide a reason for such a behaviour, we provide an additional and more detailed analysis of four functions, representative of differing behaviours in terms of power. They are: D_2z for class 1, χ^2 and Intersection for class 2, and D_2^* for class 3. We take as reference the power results in Figure 4.

In the *MR* model, Intersection shows an opposite behaviour than the expected one for $k = 10$: it has an optimal power for small values of n but it collapses to zero for n greater than 2 000 000. This drop is very well explained and exemplified by the counter-intuitive decreasing trend of the function values for $k = 10$, as it is clearly visible in the boxplots of Figure 5(b). Keeping in mind that Intersection is a similarity measure while *HD* is a distance, for the *MR*, it is evident the difference in value distributions of the former with respect to the latter. Indeed, in Figure 5(b) (*MR*), the boxplots of the former have tendency opposite to the one that a similarity measure should have, while in Figure 2, the boxplots have the correct tendency and are very well separated.

In the *MR* model, χ^2 shows a poor power for $k = 4$ independently from n while, for higher ks , a clear increasing trend is evident. This is confirmed in Figure 5(a) by the overlapping boxplots shown for $k = 4$. As in the case of Intersection, it is useful to compare those boxplot trends with the ones of *HD* in Figure 2.

D_2^* exhibits an opposite behaviour with respect to the other functions: it reaches a perfect power in the *MR* model independently from k and n , while it has poor power in the *PT* model for $k \leq 10$. This is explainable by the completely overlapping boxplots for $k = 4$ in Figure 5(c). Again, it is useful to compare those boxplot trends with the ones of *HD* in Figure 2.

D_2z is the only function that exhibits a 100% of power for $k = 8, 10$, independently from n and from the Alternative models, as confirmed in Figure 5(d). Indeed, those boxplots behave in complete analogy with the ones of *HD* displayed in Figure 2.

In conclusion, poor power or a sudden drop in power can be explained as a loss of ability of an AF function to produce values in sequence pairs generated with the Alternative models clearly disjoint from the ones produced in the case of Null model, with an increasing or decreasing trend in case of a similarity or distance function, respectively.

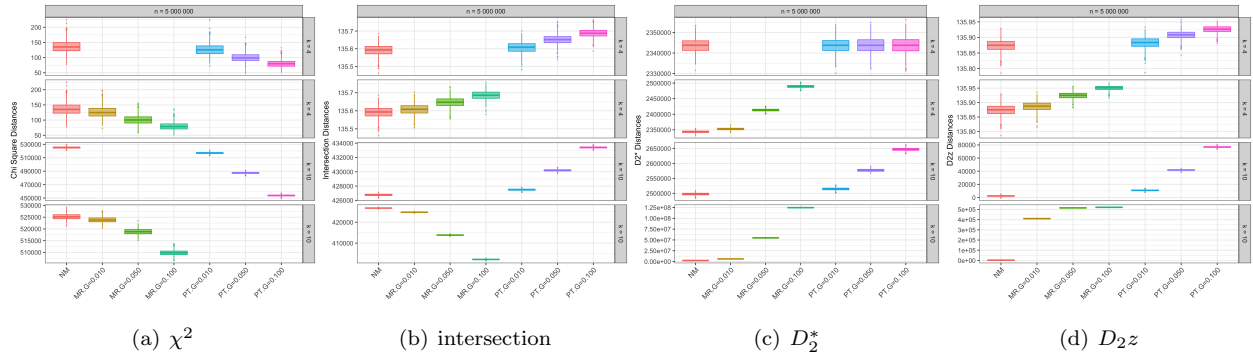


Figure 5: Separation Power results for (a) χ^2 (b) Intersection (c) D_2^* (d) D_{2z} . For each AF function, each panel corresponds to a different value of k (MR at bottom and PT at top). On the abscissa, the generative models considered, with the letter G denoting γ . For each experiment, the boxplot of the HD values computed on the corresponding set of pairs of sequences is reported on the ordinate.

4 Discussion

Our experiments, together with the analysis of the results, provide a comprehensive study of the Histogram-Based AF function performance in terms of Type I error control and power using synthetic datasets. Although empirical evaluations on gold standard real datasets are certainly appropriate for Type I error control evaluation, they are challenging in the case of power analyses as true positives (real sequence similarity) are hard to be defined.

Our results demonstrate that, although most of the tested AF functions perform well in controlling false positives, much more compelling are the results obtained in the power studies, showing different and unexpected performances.

One of the reasons for the scarce use of comparative power studies is the absence of effective computational tools. Therefore, as an additional contribution to the advancement of the State of the Art, we also provide an entire software system, based on Big Data Technologies, to rapidly carry out Power experiments.

Moreover, we get the following additional more detailed insights.

- (1) **Type I Error Control and the Choice of k .** The good performance of the selected AF functions in this setting is somewhat expected. Indeed, pragmatically, if those functions would abound in returning “false positives” then the number of studies concentrating on them would be largely unjustified. However, using a rigorous, coherent and quantitative evaluation of the proportion of false positives, we show that this proportion is not much affected by the chosen value of k , a novel and somewhat unexpected result.
- (2) **Beyond a Syntactic Grouping of AF Functions by “Family”.** Our experiments show the presence of four main AF function groups that substantially differ from the syntactic grouping provided by [11] (Figure 1, but see also [3]). We further observe that there is enough “information” regarding similarity in the k -mer statistics used by AF functions. Indeed, an alignment method such as HD and a histogram-based one such as D_{2z} have essentially the same performance. Rather, the poor performance of some measures seems to critically depend, in a non-obvious way, from the formula characterizing the function. Indeed, AF functions that are mathematically closely related, e.g., Manhattan and Canberra, may exhibit quite different power.
- (3) **The Complex and Function Specific Dependency of Power on Key AF Functions Parameters.** Based on our experiments, the ability to detect true positive similarities is deeply dependent on the value of k , the length of the sequences n and the biological reality that the generative models

are meant to encode. In particular, we note a poor power for some AF functions, even when k is selected using the already mentioned time-honored heuristic to choose k as the log of sequence length (i.e. $k = 4, 6$ for short sequences). In details, for Type I Error, the relationship between k and n seems to be irrelevant (see (1) above), while here it is AF function specific. Those findings indicate that the identification of a rule for the selection of k , even heuristic, general to all AF functions can be a very evanescent task. In this respect, our data analysis is useful to empirically guide the selection of k according to the sequence length n .

- (4) **The D_2 Family: Its Power in Relation to Alternative Models.** This is a very prominent family in Alignment-Free Computational Biology [15]. Relevant for this research is the fact that it is known that D_2^* and D_2 do not perform adequately on the *PT* model [12, 18]. Variants as a remedy to this have been proposed [10], but due to their computational cost, they are mainly of theoretic interest. We add some new facts regarding this important family. First, all of the D_2 family performs well on both models, across sequence length, but for “large” k s. Moreover, D_{2z} is the best performer on both *PT* and *MR*, for all values of k we have tested.

5 Conclusions

We have provided the first statistically sound and comprehensive study of histogram-based AF functions in terms of Type I error control and power. Our findings indicate the need to validate new AF functions via Power rather than Type I error control ones, as done so far. In this respect, we also offer software based on Big Data Technologies that make rather easy the study of new histogram-based AF functions in terms of Power. We also provide guidelines on the choice of k , a key parameter, that turns out to be function-dependent rather than “universal”. Finally, we also identify an AF function, i.e. the D_{2z} , that performs very well, across values of k , sequence lengths, and Alternative models. Despite the D_2 family, one of the most prominent AF families, has been the object of many investigations, the excellence of D_{2z} in terms of power has not been reported in previous studies.

Acknowledgements

All authors would like to thank the GARR Consortium for having made available a cutting edge OpenStack Virtual Datacenter for this research.

Funding

G.C., R.G. and U.F.P. are partially supported by GNCS Project 2019 “Innovative methods for the solution of medical and biological big data”. R.G. is additionally supported by MIUR-PRIN project “Multicriteria Data Structures and Algorithms: from compressed to learned indexes, and beyond” grant n. 2017WR7SHH. U.F.P. and F.P. are partially supported by Università di Roma - La Sapienza Research Project 2020 “Algoritmi su grafi, limitazioni nel sequenziale e opportunità nel distribuito”. C.R. is supported by the Italian Association of Cancer Research (AIRC) (grant n. IG21837).

References

- [1] S. F. Altschul, W. Gish, W. Miller, E. W. Myers, and D. J. Lipman. Basic local alignment search tool. *Journal of molecular biology*, 215(3):403–410, 1990.
- [2] G. Benoit, P. Peterlongo, M. Mariadassou, E. Drezen, S. Schbath, D. Lavenier, and C. Lemaitre. Multiple comparative metagenomics using multiset k-mer counting. *PeerJ Computer Science*, 2:1, 2016.

- [3] G. Bernard, C. X. Chan, and M. A. Ragan. Alignment-free microbial phylogenomics under scenarios of sequence divergence, genome rearrangement and lateral genetic transfer. *Scientific reports*, 6:28970, 2016.
- [4] U. Ferraro Petrillo, F. Palini, G. Cattaneo, and R. Giancarlo. Alignment-free Genomic Analysis via a Big Data Spark Platform. *Bioinformatics*, 01 2021. btab014.
- [5] R. Giancarlo, S. E. Rombo, and F. Utro. Epigenomic k-mer dictionaries: Shedding light on how sequence composition influences nucleosome positioning *in vivo*. *Bioinformatics*, 31:2939–2946, 2015.
- [6] R. Giancarlo, S. E. Rombo, and F. Utro. In vitro versus in vivo compositional landscapes of histone sequence preferences in eucaryotic genomes. *Bioinformatics*, 34:3454–3460, 2018.
- [7] G.-D. Huang, X.-M. Liu, T.-L. Huang, and L.-C. Xia. The statistical power of k-mer based aggregative statistics for alignment-free detection of horizontal gene transfer. *Synthetic and Systems Biotechnology*, 4:150–156, 2019.
- [8] G.-D. Huang, X.-M. Liu, T.-L. Huang, and L.-C. Xia. The statistical power of k-mer based aggregative statistics for alignment-free detection of horizontal gene transfer. *Synthetic and Systems Biotechnology*, 4:150 – 156, 2019.
- [9] A. Jain and R. Dubes. *Algorithms for Clustering Data*. Prentice-Hall, Engelwood Cliffs, 1988.
- [10] X. Liu, L. Wan, J. Li, G. Reinert, M. S. Waterman, and F. Sun. New powerful statistics for alignment-free sequence comparison under a pattern transfer model. *Journal of theoretical biology*, 284:106–116, 2011.
- [11] B. B. Luczak, B. T. James, and H. Z. Girgis. A survey and evaluations of histogram-based statistics in alignment-free sequence comparison. *Briefings in Bioinformatics*, 20(4):1222–1237, 12 2017.
- [12] G. Reinert, D. Chew, F. Sun, and M. S. Waterman. Alignment-free sequence comparison (I): statistics and power. *Journal of Computational Biology*, 16(12):1615–1634, 2009.
- [13] T. F. Smith and M. S. Waterman. Identification of common molecular subsequences. *Journal of molecular biology*, 147(1):195–197, 1981.
- [14] K. Song, J. Ren, G. Reinert, M. Deng, M. S. Waterman, and F. Sun. New developments of alignment-free sequence comparison: measures, statistics and next-generation sequencing. *Briefings in Bioinformatics*, 15(3):343–353, 09 2013.
- [15] K. Song, J. Ren, G. Reinert, M. Deng, M. S. Waterman, and F. Sun. New developments of alignment-free sequence comparison: measures, statistics and next-generation sequencing. *Briefings in Bioinformatics*, 15:343–353, 2013.
- [16] F. Utro, D. E. Platt, and L. Parida. A quantitative and qualitative characterization of k-mer based alignment-free phylogeny construction. In M. Bartoletti, A. Barla, A. Bracciali, G. W. Klau, L. Peterson, A. Policriti, and R. Tagliaferri, editors, *Computational Intelligence Methods for Bioinformatics and Biostatistics*, pages 19–31, Cham, 2019. Springer International Publishing.
- [17] S. Vinga and J. Almeida. Alignment-free sequence comparison - a review. *Bioinformatics*, 19:513–523, 2003.
- [18] L. Wan, G. Reinert, F. Sun, and M. S. Waterman. Alignment-free sequence comparison (II): theoretical power of comparison statistics. *Journal of Computational Biology*, 17:1467–1490, 2010.
- [19] A. Zielezinski, H. Z. Girgis, G. Bernard, C.-A. Leimeister, K. Tang, T. Dencker, A. K. Lau, S. Röhling, J. J. Choi, M. S. Waterman, M. Comin, S.-H. Kim, S. Vinga, J. S. Almeida, C. X. Chan, B. T. James, F. Sun, B. Morgenstern, and W. M. Karlowski. Benchmarking of alignment-free sequence comparison methods. *Genome Biology*, 20(1):144, 2019.

The Power of Alignment-Free Histogram-based Functions: a Comprehensive Genome Scale Experimental Analysis

Supplementary Material

Giuseppe Cattaneo^{*†} Umberto Ferraro Petrillo[‡] Raffaele Giancarlo[§]
Francesco Palini[‡] Chiara Romualdi[¶]

Abstract

Additional details about the Main Manuscript are provided in this document.

1 Distance Functions

In this section, we provide definitions of the AF functions included in this study. In what follows, we adopt both the classification and the notation from [1]. It is to be remarked that some of the AF functions defined next appear in the Literature with different names or they are easy variants of the functions introduced here. For instance, FFP adopted in [3] is the well known Jensen-Shannon Divergence defined here. For the interested reader, the original publication where the functions defined here have been introduced can be found in [1] for the less known cases.

Given a set of sequences $S = \{s_1, \dots, s_n\}$, a k -mer histogram h_s for a sequence s in the set is defined as follows:

$$h_s = \langle c(w_1), c(w_2), \dots, c(w_{|K|}) \rangle \quad (1)$$

where $c(w_i)$ is the number of occurrences of the word w_i (i.e. the i -th k -mer) in the sequence s and K is the set of all possible words of length k over the alphabet $\{A, C, G, T\}$.

1.1 The Minkowski Family

Given two sequences s and t and their associated statistics h_s and h_t , the *Euclidean* distance is defined as:

$$Euclidean(h_s, h_t) = \sqrt{\sum_{w \in K} (h_s(w) - h_t(w))^2} \quad (2)$$

A widely adopted variant of the *Euclidean* distance is the *Manhattan* distance:

$$Manhattan(h_s, h_t) = \sum_{w \in K} |h_s(w) - h_t(w)| \quad (3)$$

^{*}Dipartimento di Informatica, Università di Salerno, Fisciano (SA), 84084, Italy

[†]To whom correspondence should be addressed.

[‡]Dipartimento di Scienze Statistiche, Università di Roma - La Sapienza, Rome, 00185, Italy

[§]Dipartimento di Matematica ed Informatica, Università di Palermo, Palermo, 90133, Italy

[¶]Dipartimento di Biologia, Università di Padova, Padova, 35131, Italy.

Another member of this family, the *Chebyshev* distance, is based on the idea of applying the p -th root on the *Manhattan* distance, with $p \rightarrow \infty$, and it is defined as follows:

$$Chebyshev(h_s, h_t) = \max_{w \in K} |h_s(w) - h_t(w)| \quad (4)$$

1.2 The χ^2 Distance

It is defined as:

$$\chi^2(h_s, h_t) = \sum_{w \in K} \frac{(h_s(w) - h_t(w))^2}{(h_s(w) + h_t(w))} \quad (5)$$

1.3 The Canberra Distance

It is a mix between Manhattan and χ^2 distances:

$$Canberra(h_s, h_t) = \sum_{w \in K} \frac{|h_s(w) - h_t(w)|}{(h_s(w) + h_t(w))} \quad (6)$$

1.4 The D_2 Statistics

It expresses the similarity of two sequences in a very natural way as a sort of inner product between two histograms as shown in equation (7).

$$D_2(h_s, h_t) = \sum_{w \in K} h_s(w)h_t(w) \quad (7)$$

However, extensive studies of this function suggest that a standardized version of it is more useful in the AF sequence analysis setting. Such a variant is denoted D_2^Z . It is as D_2 , except that the histograms have been standardized via the well known z-score transformation. Details can be found in [1].

We also consider two other members of the D_2 family, denoted D_2^S and D_2^* and described in [4].

D_2^S is based on the finding [2] that if two independent random variables X and Y are normally distributed with mean zero, also $\frac{XY}{\sqrt{X^2+Y^2}}$ is normally distributed. We normalize $h_s(w)$ and $h_t(w)$ as follow:

$$\tilde{h}_s(w) = h_s(w) - np_s(w)$$

and

$$\tilde{h}_t(w) = h_t(w) - mp_t(w)$$

In which n and m are the number of k -mers, respectively, in S and T , while $p_s(w)$ and $p_t(w)$ are the probabilities of the k -mer w under the background model for, respectively, S and T .

The D_2^S statistics is defined as follow:

$$D_2^S = \sum_{w \in K} \frac{\tilde{h}_s(w)\tilde{h}_s(w)}{\sqrt{\tilde{h}_s(w)^2 + \tilde{h}_s(w)^2}} \quad (8)$$

The D_2^* statistic is based on the idea that, for relatively long k -mers, the number of occurrences can be approximated by a Poisson distribution, thus mean and variance are nearly the same.

The D_2^* statistics is defined as follow:

$$D_2^* = \sum_{w \in K} \frac{\tilde{h}_s(w)\tilde{h}_s(w)}{\sqrt{np_s(w)mp_t(w)}} \quad (9)$$

1.5 The Intersection Family

From this family, we selected two distances. The first is the *Intersection* distance, also known as *Czekanowski*, is based on the intersection of the k -mers counts divided by their union. It is:

$$Intersection(h_s, h_t) = \sum_{w \in K} \frac{2 * \min(h_s(w), h_t(w))}{h_s(w) + h_t(w)} \quad (10)$$

The second is the *Kulczynski2* distance;

$$Kulczynski2(h_s, h_t) = A_\mu \sum_{w \in K} \min(h_s(w), h_t(w)) \quad (11)$$

where A_μ is equal to $\frac{4^k(\mu_s - \mu_t)}{2\mu_s\mu_t}$ (μ_s and μ_t denote the mean of the histograms h_s and h_t , respectively).

1.6 The Inner Product Family

The *Harmonic Mean* distance is:

$$HarmonicMean(h_s, h_t) = 2 \sum_{w \in K} \frac{h_s(w)h_t(w)}{h_s(w) + h_t(w)} \quad (12)$$

As opposed to the Euclidean distance that computes the square root over the summation value, the *Squared Chord* computes the square root over each value of the histograms independently:.

$$SquaredChord(h_s, h_t) = \sum_{w \in K} \left(\sqrt{h_s(w)} - \sqrt{h_t(w)} \right)^2 \quad (13)$$

This can be simplified as

$$= \sum_{w \in K} h_s(w) + h_t(w) - 2\sqrt{h_s(w)h_t(w)} \quad (14)$$

1.7 The Divergence Family

This family uses probabilities to compare two sequences measuring the distance in the log-probability space. From such a family, we selected the *Jeffrey* and the *Jensen-Shannon* distances. The former is defined as:

$$Jeffrey(h_s, h_t) = \sum_{w \in K} (p_s(w) - p_t(w)) \ln \frac{p_s(w)}{p_t(w)} \quad (15)$$

while the second (JSD for short) is defined in 16:

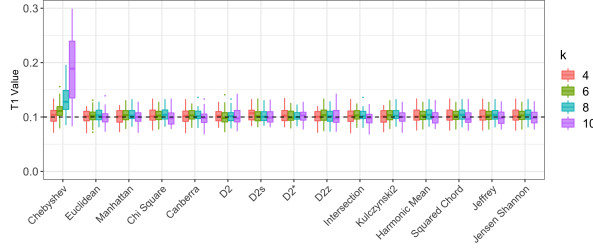
$$\begin{aligned} JSD(h_s, h_t) &= \frac{1}{2} \sum_{w \in K} p_s(w) \log_2 \left(\frac{p_s(w)}{\frac{1}{2}(p_s(w) + p_t(w))} \right) \\ &\quad + \frac{1}{2} \sum_{w \in K} p_t(w) \log_2 \left(\frac{p_t(w)}{\frac{1}{2}(p_s(w) + p_t(w))} \right) \end{aligned} \quad (16)$$

where $p_s(w)$ is the empirical probability of k -mer w over all the strings of length k from the alphabet $\{A, C, G, T\}$ in the input sequence s and therefore $p_s(w) = \frac{h_s(w)}{4^k}$.

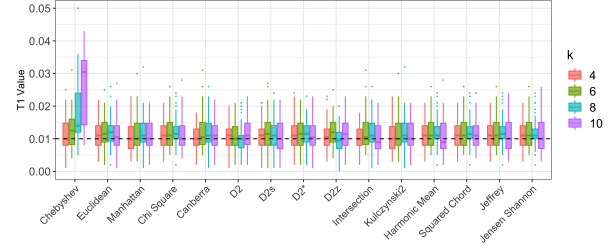
2 Results: Additional Material

2.1 Type I error control: additional figures

Here we report additional figures with respect to Section 3.1 of the main text, i.e., Figure 1.



(a) $\alpha=0.10$



(b) $\alpha=0.01$

Figure 1: Results of the T1 Error Control experiments, for nominal levels 0.10 (left panel) and 0.01 (right panel). The dotted black line corresponds to the nominal level.

2.2 Ability to Capture Similarity Trends: additional figures

Here we report additional figures with respect to Section 3.2, i.e., Figures 2 - 3.

2.3 Power Estimation: additional figures

Here we report an additional figure with respect to Section 3.3, i.e., Figure 4.

2.4 Insights into the power of AF functions: additional figures

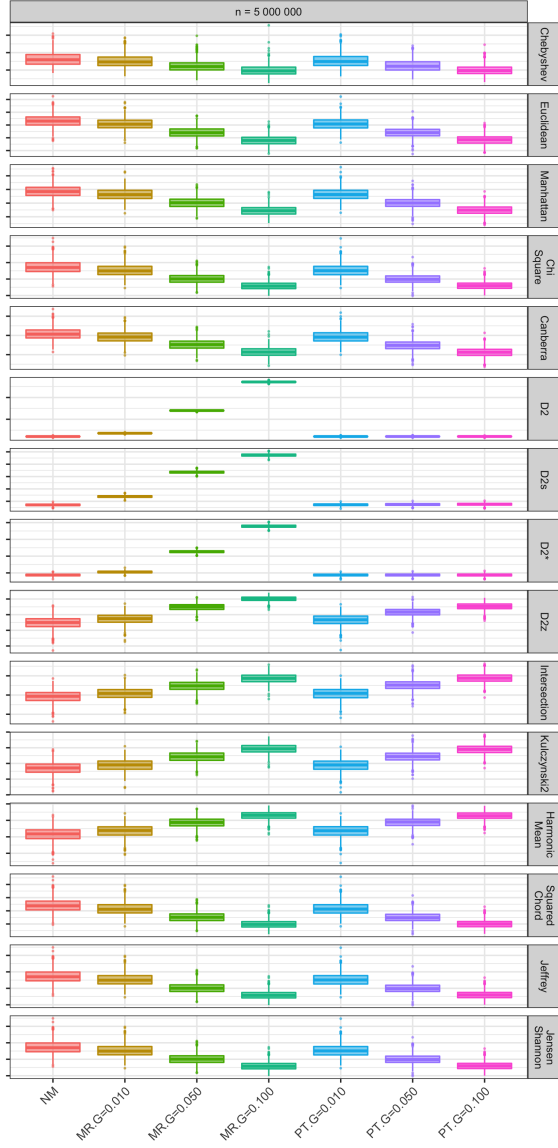
Here we report additional figures with respect to Section 3.3.2, i.e., Figures 2 - 3.

Acknowledgements

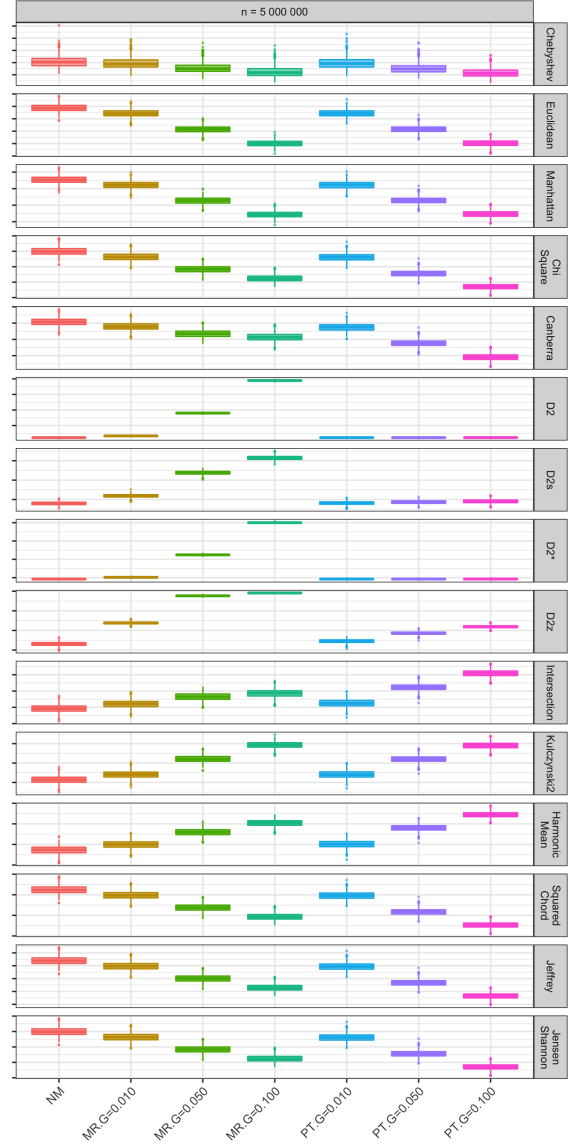
All authors would like to thank the GARR Consortium for having made available a cutting edge OpenStack Virtual Datacenter for this research.

Funding

G.C., R.G. and U.F.P. are partially supported by GNCS Project 2019 “Innovative methods for the solution of medical and biological big data”. R.G. is additionally supported by MIUR-PRIN project “Multicriteria Data Structures and Algorithms: from compressed to learned indexes, and beyond” grant n. 2017WR7SHH. U.F.P. and F.P. are partially supported by Università di Roma - La Sapienza Research Project 2020 “Algoritmi su grafi, limitazioni nel sequenziale e opportunità nel distribuito”. C.R. is supported by the Italian Association of Cancer Research (AIRC) (grant n. IG21837).

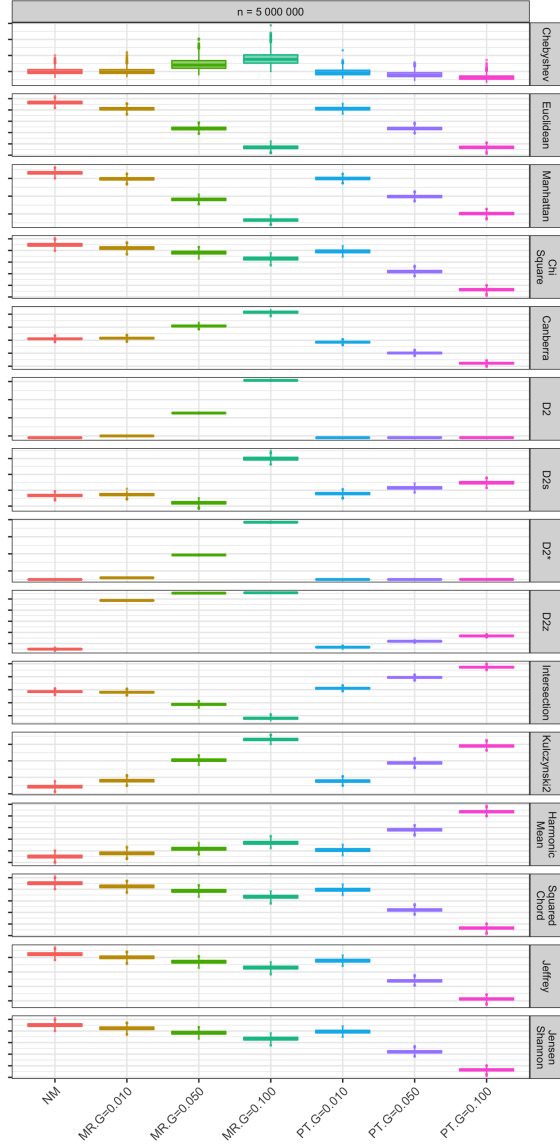


(a) $k=4$

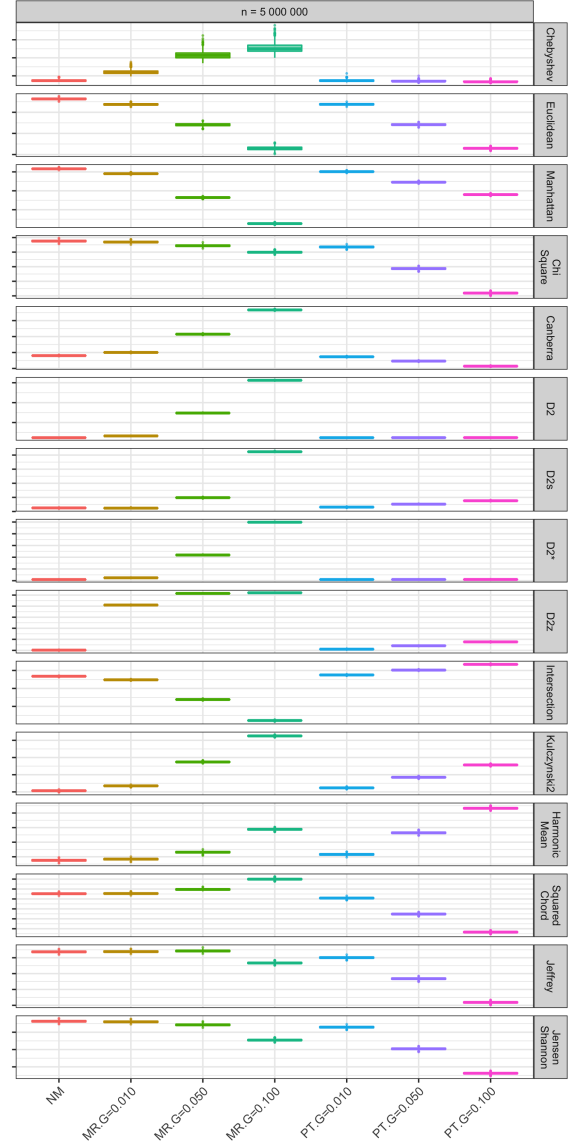


(b) $k=6$

Figure 2: Separation, graphical view, of the AF function values for all measures and for $n = 5\,000\,000$ and $k = 4$ (left panel) and $k = 6$ (right panel). AF function names are on the right of each boxplot experiment. The remaining part of the legend is as in Figure 2 as in the Main Text.



(a) $k=8$



(b) $k=10$

Figure 3: Separation, graphical view, of the AF function values for all measures and for $n = 5\,000\,000$ and $k = 8$ (left panel) and $k = 10$ (right panel). AF function names are on the right of each boxplot experiment. The remaining part of the legend is as in Figure 2 as in the Main Text.

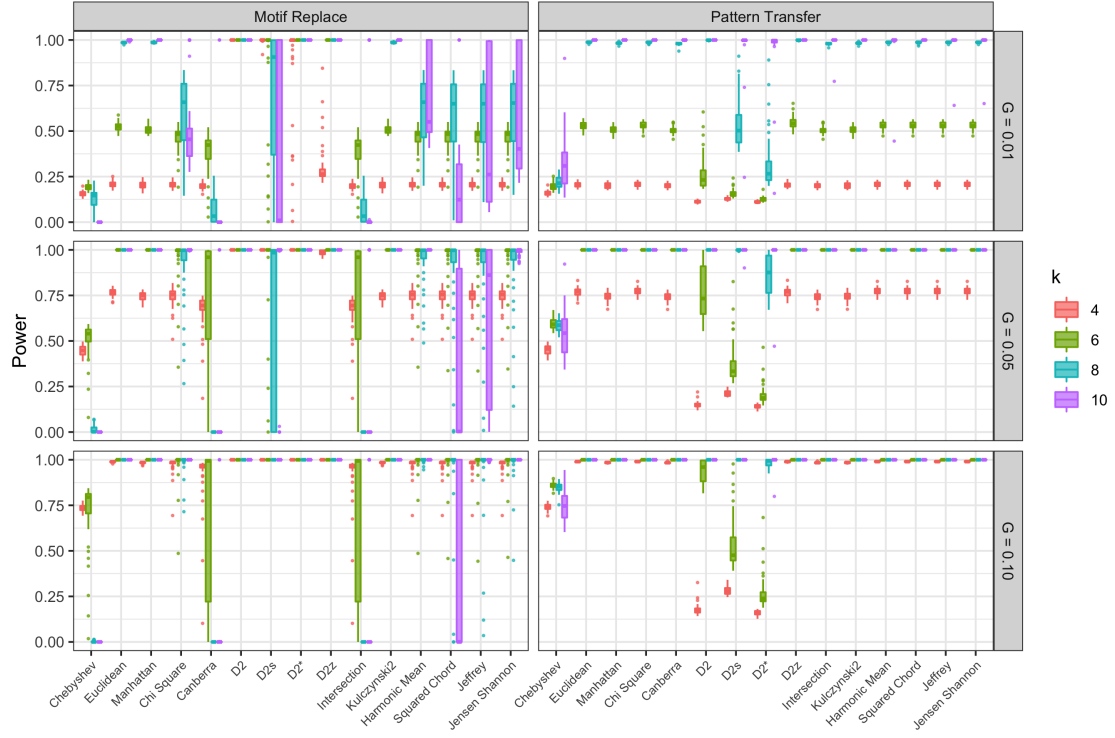


Figure 4: Distribution of the proportion of true positives cumulatively by length, for each AF and $\gamma = 0.01, 0.05, 0.1$, for both Alternative Models, represented by boxplots colored according to k .

References

- [1] B. B. Luczak, B. T. James, and H. Z. Girgis. A survey and evaluations of histogram-based statistics in alignment-free sequence comparison. *Briefings in Bioinformatics*, 20(4):1222–1237, 12 2017.
- [2] L. Shepp. Normal functions of normal random variables. *Siam Review*, 4(3):255, 1962.
- [3] G. E. Sims and S.-H. Kim. Whole-genome phylogeny of *Escherichia coli*/Shigella group by feature frequency profiles (FFPs). *Proceedings of the National Academy of Sciences*, 108(20):8329–8334, 2011.
- [4] K. Song, J. Ren, G. Reinert, M. Deng, M. S. Waterman, and F. Sun. New developments of alignment-free sequence comparison: measures, statistics and next-generation sequencing. *Briefings in Bioinformatics*, 15:343–353, 2013.